Environmental Science & Technology

pubs.acs.org/est

Article

Distinct Ultrafine Particle Profiles Associated with Aircraft and Roadway Traffic

Elena Austin,* Jianbang Xiang, Timothy R. Gould, Jeffry H. Shirai, Sukyong Yun, Michael G. Yost, Timothy V. Larson, and Edmund Seto

Cite This: *Environ. Sci. Technol.* 2021, 55, 2847−2858

Read Online

ACCESS | Metrics & More | Article Recommendations | Supporting Information

ABSTRACT: The Mobile ObserVations of Ultrafine Particles study was a two-year project to analyze potential air quality impacts of ultrafine particles (UFPs) from aircraft traffic for communities near an international airport. The study assessed UFP concentrations within 10 miles of the airport in the directions of aircraft flight. Over the course of four seasons, this study conducted a mobile sampling scheme to collect time-resolved measures of UFP, CO_2, and black carbon (BC) concentrations, as well as UFP size distributions. Primary findings were that UFPs were associated with both roadway traffic and aircraft sources, with the highest UFP counts found on the major roadway (I-5). Total concentrations of UFPs alone (10−1000 nm) did not distinguish roadway and aircraft features. However, key differences existed in the particle size distribution and the black carbon concentration for roadway and aircraft features. These differences can help distinguish between the spatial impact of roadway traffic and aircraft UFP emissions using a combination of mobile monitoring and standard statistical methods.

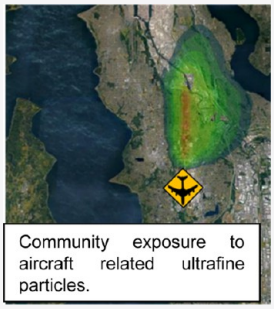

1. INTRODUCTION

The health effects associated with $PM_{2.5}$ [particles with diameters less than 2.5 μm (μm)] mass concentrations have been well studied, leading to established standards and routine monitoring.[1] However, $PM_{2.5}$ consists of a mixture of particles of varying sizes from a variety of sources, with the most numerous particles by count usually falling within the ultrafine size range (<100 nm). Typical reported urban background concentrations of ultrafine particles (UFPs), ranging from 5000 to 40,000 particles/cubic centimeter (#/cm^3), are impacted by weather and proximity to roadways and airports.[2−11] The total mass concentration associated with these UFPs is typically less than 2 μg/m^3. Thus, the UFP is not considered an important contributor to the mass of $PM_{2.5}$. In the ambient environment, the spatial and temporal variation of UFPs tends to differ significantly from that of $PM_{2.5}$ or PM_{10}.[12]

Early toxicological studies suggested that UFPs may be more relevant to health than larger-sized particles due to the larger surface area relative to the mass of UFPs and the ability for smaller sized particles to penetrate within the body.[13,14] While the epidemiologic evidence for UFP health effects is still limited, there exist some studies to inform quantitative concentration−response functions for all-cause mortality,[15] and recent large epidemiologic studies have considered UFP exposure estimates for a variety of outcomes, including breast cancer,[16] ischemic heart disease,[17−21] prostate cancer,[22] asthma, and COPD.[23]

Although much research on environmental variations in UFP concentrations has focused on roadway vehicle emissions of UFPs,[10,24−30] recent research identifies a previously underappreciated source of UFPs, which may be responsible for large population exposures globally. Monitoring campaigns conducted in communities near the Los Angeles,[31−33] Atlanta,[34] Boston,[35,36] New York,[37] and Amsterdam[38] airports have all identified elevated levels of total UFPs in proximity to international airports. The work in LAX demonstrated significant downwind exposures (~10 km) of UFP but did not have information on upwind community exposures.[35,39] This has led to difficulty in determining community impacts and differential exposures during aircraft takeoffs versus landings. Previous work, using near-source fixed-site sampling at one location[38,40] or nonsimultaneous upwind and downwind locations, has not yielded consistent results with respect to the relative impact of landing versus takeoff flight activity.[41] Previous work has highlighted the compositional differences between aircraft and roadway traffic sources,[37,40,42−45] as well as documenting uniquely different fuel-based emissions of roadway and roadway traffic-based sources.[39] To our knowledge, exploiting these known differences to derive spatially resolved exposures zones within a mobile monitoring framework is unique to the work presented here.

The Mobile ObserVations of Ultrafine Particles (MOV-UP) study[45] was a two-year project, funded by the State of

Received: September 3, 2020
Revised: January 12, 2021
Accepted: January 13, 2021
Published: February 5, 2021

https://dx.doi.org/10.1021/acs.est.0c05933
Environ. Sci. Technol. 2021, 55, 2847−2858

Washington, aiming to study air quality impacts of air traffic for communities located near and below the flight paths of the Seattle-Tacoma International (Sea-Tac) Airport. The study assessed UFP concentrations within 10 miles upwind and downwind of the airport under the flight trajectories. The goals of this study were to demonstrate the ability to distinguish between aircraft and other sources of UFPs and compare levels of UFPs in areas impacted by high volumes of air traffic with those areas that are much less impacted.

To our knowledge, this work is significant and novel in that:

1 mobile monitoring was simultaneously performed at a significant distance (~10 km) both upwind and downwind of a major airport to examine the relative impacts of takeoffs versus landings (Stacey et al.[40] and Keuken et al.[38] used near-source fixed-site sampling at one location coupled with the wind direction; Lopes et al.[41] used fixed-site sampling at both locations but did not sample simultaneously upwind and downwind; and Shirmohammadi et al.[39] and Hudda et al.[33] did not sample upwind at LAX);

2 multivariate analysis was conducted on purely mobile monitoring data to separate traffic sources from aircraft sources (Tessum et al.[42] conducted PCA in the Los Angeles study, but relied on both mobile and fixed-site data; others using only fixed-site data include Rivas et al.[43] and Masiol et al.,[37,44] who conducted PMF and analyses on fixed-site data); and

3 PCA-based predictions were used to derive spatially resolved independent estimates of fuel-based emission factors (Shirmohammadi et al.[39] assessed emissions based on a more spatially limited sampling scheme), demonstrating clear separation in emissions between roadway traffic and aircraft, as well as between landing and takeoff conditions.

2. METHODS

Sampling for the MOV-UP study was conducted seasonally from February 2018 through March 2019. The study was conducted using a mobile sampling design, with two hybrid-electric vehicles equipped with sampling instruments and an isokinetic probe, which sampled ambient air as the vehicles moved through defined routes. All measurements were conducted after an initial vehicle warmup period of at least 30 min. This sampling platform has been previously described in detail.[29]

2.1. Study Area. The study domain included the areas to the north and south of the Sea-Tac International Airport. Mobile monitoring occurred along defined routes termed *transects*, which were designed to sample perpendicular to the flight path in an east-west direction at fixed latitudes north and south of the airport.

Because of terrain and roadway considerations, some transects deviated slightly from the target latitude. We monitored transects 10 miles north (five transects) and 10 miles south (six transects) of the airport (Figure S1, Supporting Information). The campaign was designed to capture multiple repeated samples of each transect. Please see a summary description of each route in the Supporting Information, Table S1.

Sampling occurred during the mid-day and afternoon hours to increase comparability between the different sampling repeats and to minimize the effect of a changing height of the atmospheric mixing layer. In the interest of decreasing confounding by weather patterns and other time-varying changes in UFP concentration, most sampling days consisted of two simultaneous sampling vehicles north and south of the airport.

2.2. Mobile Monitoring Measurements. A detailed description of the mobile platform is given elsewhere.[29] In summary, each mobile monitoring platform consisted of a Toyota Prius hybrid-electric vehicle from University of Washington Fleet Services and several portable monitors for air pollution measurements.

Location and speed were captured using a GPS logger on the dash of the vehicle. The sampling inlet was mounted on the roof of the vehicle pointing forward and positioned above the vehicle boundary layer, the zone of turbulence directly associated with vehicle motion. Airflow entered the vehicle through the otherwise sealed left rear window from where they were connected to the instruments. Particle loss was minimized using stainless steel, copper, and conductive flexible tubing for the particle sampling inlet and connecting tubing. The exhaust pipe from the vehicle's gasoline engine was discharged on the right side low to the ground, away from the elevated, left-side air monitoring inlet. To further minimize the potential for self-pollution, the vehicle's gasoline engine would typically shut off when stopped at red traffic lights.

As summarized in Table S2, each mobile platform was equipped with a CPC (model 3007, TSI Inc., MN), two P-Trak (model 8525, TSI Inc., MN) condensation nucleus particle counters (one with inlet diffusion screens to increase the minimum detected particle size), a black carbon aerosol monitor (microAeth AE51, AethLabs, CA), a CO_2 analyzer (Li-850, LI-COR, NE), and a GPS receiver (DG-500, GlobalSat WorldCom Corporation, TW). Additionally, a NanoScan SMPS nanoparticle sizer (model 3910, TSI Inc., MN) was rotated between the two platforms. All these instruments measured and recorded data at one-second intervals except the NanoScan (1 min intervals).

2.3. Flight and Meteorological Data. We requested flight data from the Federal Aviation Administration (FAA) western regional office using a data-disclosure request. The data covered 2018 and included track data for all the flights in the Seattle metropolitan region. The density of flights with an altitude of lower than 750 m was gridded in cells of 70 × 100 m by hour of the year for the study domain. We used the single-aircraft track data to calculate the predominant landing direction and the number of flights landing per hour. The flight data included flights arriving and departing from all local airports.

The Washington Automated Surface Observing System (ASOS) network[46] provided us with wind speed and direction, temperature, and relative humidity based on 15 min data from Sea-Tac.

2.4. Instrument Calibration and Colocation. All instruments were calibrated for flow, zero, and span in the factory before we received them. The full calibration process is described in detail elsewhere.[47] The Li-850 CO_2 analyzer was calibrated for zero and span in the lab with certified standard CO_2 gas. We conducted mobile colocation with all sets of UFPs and/or BC monitors deployed in one vehicle, using the average reading of all instruments as a reference. Since there are no traceable standards for calibration of UFPs and BC monitors, we used the averaged measured results of all sets of duplicate monitors as the reference. See Table S3 for the

https://dx.doi.org/10.1021/acs.est.0c05933
Environ. Sci. Technol. 2021, 55, 2847−2858

summary of calibration coefficients and R^2. Note that five P-Trak monitors, four P-Trak screened monitors, two CPC monitors, and three AE51 monitors were rotated between the two vehicles.

2.5. Data Integration. At the end of each sampling day, we collected raw data from each instrument on a secure server. There were 2,876,538 individual time points collected. We developed a merging script to

1 compute 30 s center-aligned rolling means to smooth concentrations of CO_2 and 1 s particle numbers;
2 smooth the BC data using an optimized noise-reduction averaging (ONA) algorithm (with the attenuation coefficient (ATN) threshold set to ΔATN = 0.06) to reduce potential instrumental optical and electronic noise;[48]
3 apply a common 1 min time basis for all sampling instruments;
4 calculate short-term 30 min background concentrations for black carbon and particle count, based on the method presented elsewhere;[29]
5 apply between-instrument calibration factors as discussed in the "Quality Control" section; and finally,
6 merge meteorological parameters and flight data per 1 h metric.

2.6. Quality Control. We also performed data quality control and applied the following criteria. We first excluded GPS coordinates from the analysis which were outside of the study zone presented in Figure S1. We flagged them as erroneous zero readings across all NanoScan 60 s samples (57 measurements). We excluded data with black carbon concentrations exceeding 27,000 ng/m^3 (0.01% of the data). We based one of our particle metrics between 10 and 20 nm on the difference in short-term measures of the CPC and P-Trak instruments. In instances where this difference was negative (<1.2% of the collected data), we replaced the negative value with a random normal distribution of data centered around 1 particle/cm^3, eliminating negative values in the data. The maximum negative difference before this transformation was −32, the mean was −0.25, and the median was −0.11. Next, automated flagging routines censored data corresponding to instrument error codes and instruments operating out of specified parameters or data otherwise missing (instrument rebooted itself, lost power, etc.). We then manually inspected the time series for each pollutant for anomalies and cross-checked with field technician notes. Finally, we combined the resulting mobile monitoring data into a final data file. All data management was performed in R version 3.5.1.

2.7. Descriptive Statistics. We computed descriptive statistics of the collected data including mean, median, interquartile range, and range and performed graphical representation of the data using the ggplot2 library in R.

We calculated some informative pollutant ratios for descriptive purposes. These measures are based on differences in the cut point of the CPC, Ptrak, and screened PTrak instruments. To potentially account for the prevalence of various particle sizes and contribution of black carbon soot originating from different emission source types, we computed ratios for the proportion of 10−20 nm particles relative to total measured particles, the proportion of 20−36 nm particles relative to total measured particles, and the proportion of 10−20 nm particles to black carbon concentration.

Also, we calculated the concentration of particles above the background concentration of total particles as the quantity above the 5th percentile of the 30 min concentration of particles. This approach has been successfully employed in previous mobile monitoring campaigns to account for neighborhood-level concentrations.[26,34]

2.8. Principal Component Analysis. Principal component analyses (PCA) were performed using the "psych" and "GPA rotation" packages in R. Factors with eigenvalues greater than 1 being retained and a Varimax rotation applied to improve factor interpretability.

Input variables beyond the directly measured variables were included in the PCA analysis to capture a variety of composition and size information on the particles collected over the mobile monitoring campaign. These are described in the Descriptive Statistics section.

A sensitivity analysis was developed based on a subset of the data containing NanoScan data. This second PCA solution was used to interpret and validate the full model. Results of the two PCA analyses were compared using both correlations of the scores and composition information. Principal component features were interpreted based on composition and spatially described based on GPS data collected during the mobile monitoring drives.

2.9. Spatial Mapping. We performed mapping of pollutants, principal components, and flight patterns on a grid of 0.001 degrees of longitude (∼70 m) and 0.002 degrees of latitude (∼100 m). We represented the distribution of pollutant concentrations on a quantile scale and performed plotting using the R implementation of the leaflet JavaScript tool.

2.10. Fuel-Based Emission Factors. Fuel-based emissions factors are typically computed as a concentration of emissions produced per gram of fuel burned. The emission factor of particular interest in this study is the very smallest range of UFPs that we termed "ultra-ultrafine particles" (Ultra-UF), defined by eq 1

$$\text{emission factor (EF)} = \frac{\#\text{ of ultra-UF particles (10 − 20 nm)}}{\text{fuel (kg)}} \quad (1)$$

We do not know the total kilograms of fuel burned for the traffic and aircraft sources. However, we can use the change in measured ambient CO_2 concentration over a short period as a proxy for changes in fuel consumption. The change in CO_2 relates to fuel consumption by estimating the weight fraction of carbon (ω_c) in the traffic and aircraft fuel. We reported these weights in the literature measuring between 0.85 and 0.87 for traffic and 0.86 for Jet A fuel.[49]

Based on a previously developed method,[39] we estimated the fuel-based emissions factors (eq 2) for quantiles of locations we identified as "high aircraft impact" and "high traffic impact" through the PCA analysis. Urban background concentrations are defined as the 5th percentile of the data collected during each hour of monitoring,[26,29] for both the Ultra-UF and CO_2 concentrations.

$$EF_P = \left(\frac{[P]_i - [P]_{bg}}{[CO_2]_i - [CO_2]_{bg}}\right)\omega_c \times \alpha \quad (2)$$

where $[P]_i$ represents the concentration of Ultra-UF particles at the impact area (#/cm^3); $[P]_{bg}$ represents the hourly

https://dx.doi.org/10.1021/acs.est.0c05933
Environ. Sci. Technol. 2021, 55, 2847−2858

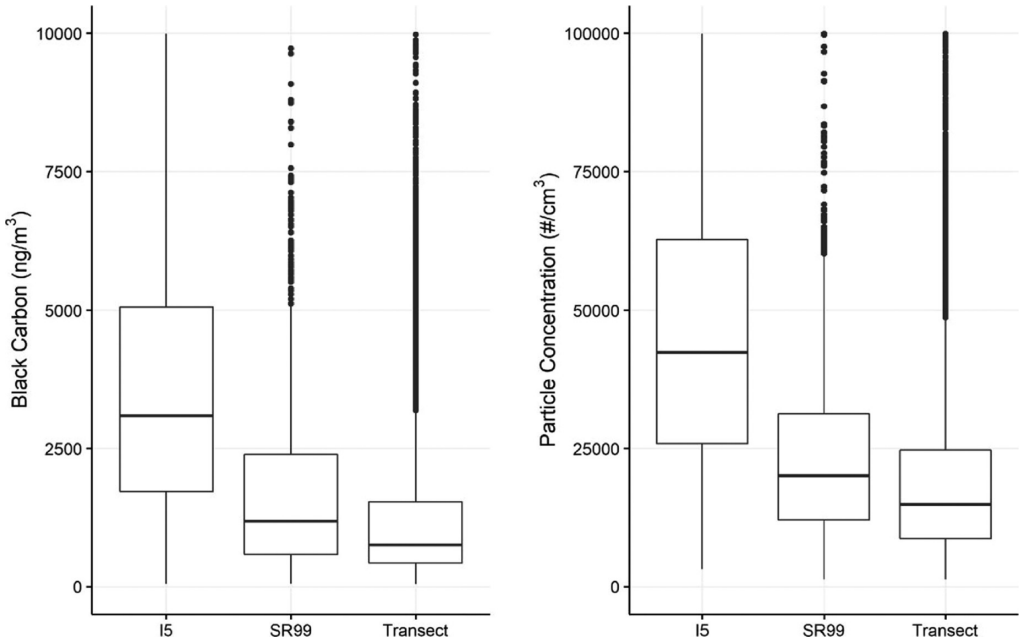

Figure 1. Major roadway (Interstate 5 and State Route 99) and mobile monitoring transect concentrations of traffic-related pollutants: (A) black carbon mass and (B) total particle (>10 nm) number. This figure includes all the data collected on all transects north and south of the airport.

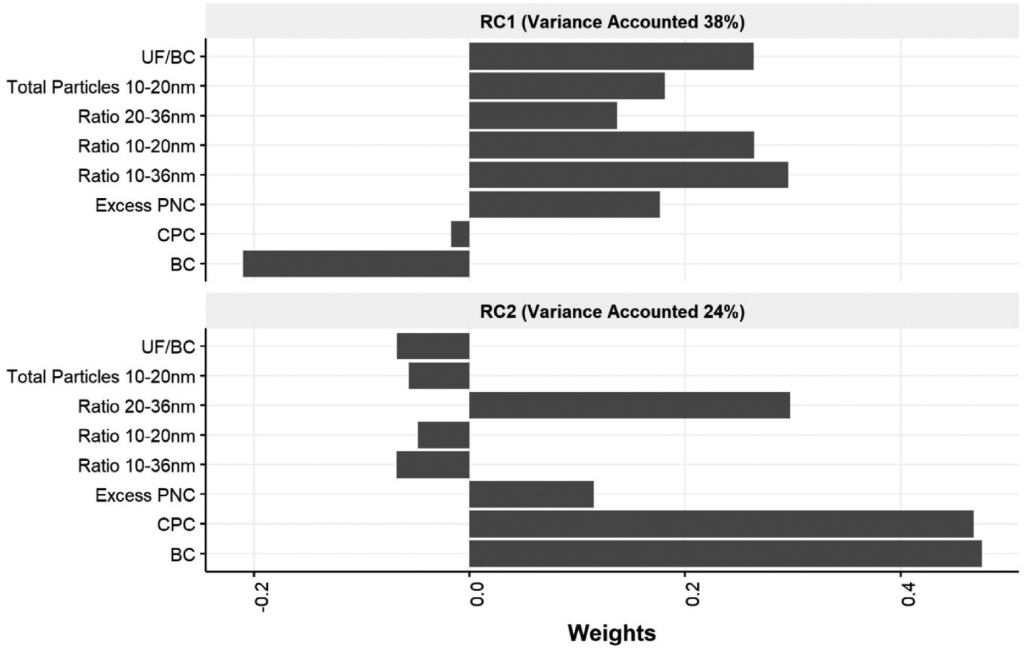

Figure 2. Principal component factor loadings for each feature.

background concentration of Ultra-UF particles (#/cm^3); $[CO_2]_i$ represents the concentration of CO_2 at the impact area (g/m^3); $[CO_2]_i$ represents the hourly background concentration of CO_2 (kg/m^3); ω_c is the weight fraction of traffic and aircraft fuel; and α is the unit conversion factor (10^{15}). The nonparametric Wilcoxon rank sum test was used for comparison of EF between different locations and landing conditions.

3. RESULTS

3.1. Descriptive Summary. We conducted mobile monitoring with either one or two vehicles for 63 days during the time domain of our study between February 7, 2018, and January 11, 2019. Typically, the two vehicles were sampled for 5 h within the interval from approximately 11:00 to 17:00 on different routes—either along five transects to the north or along five transects (or six during the summer season) to the south of Sea-Tac. Overall, the airport was in south flow operation (planes taking off to the south and landing from the north), 67% of our sampling times. This is comparable to the overall yearly proportion of the south flow operation of 65% (Table S4). The wind-rose plots (Figure S2) are separated by north and south flow operating conditions derived from the flight-track data. As expected, during north flow operation, winds are predominantly from the north and northwest, whereas during south flow operation, winds are from the south

https://dx.doi.org/10.1021/acs.est.0c05933
Environ. Sci. Technol. 2021, 55, 2847−2858

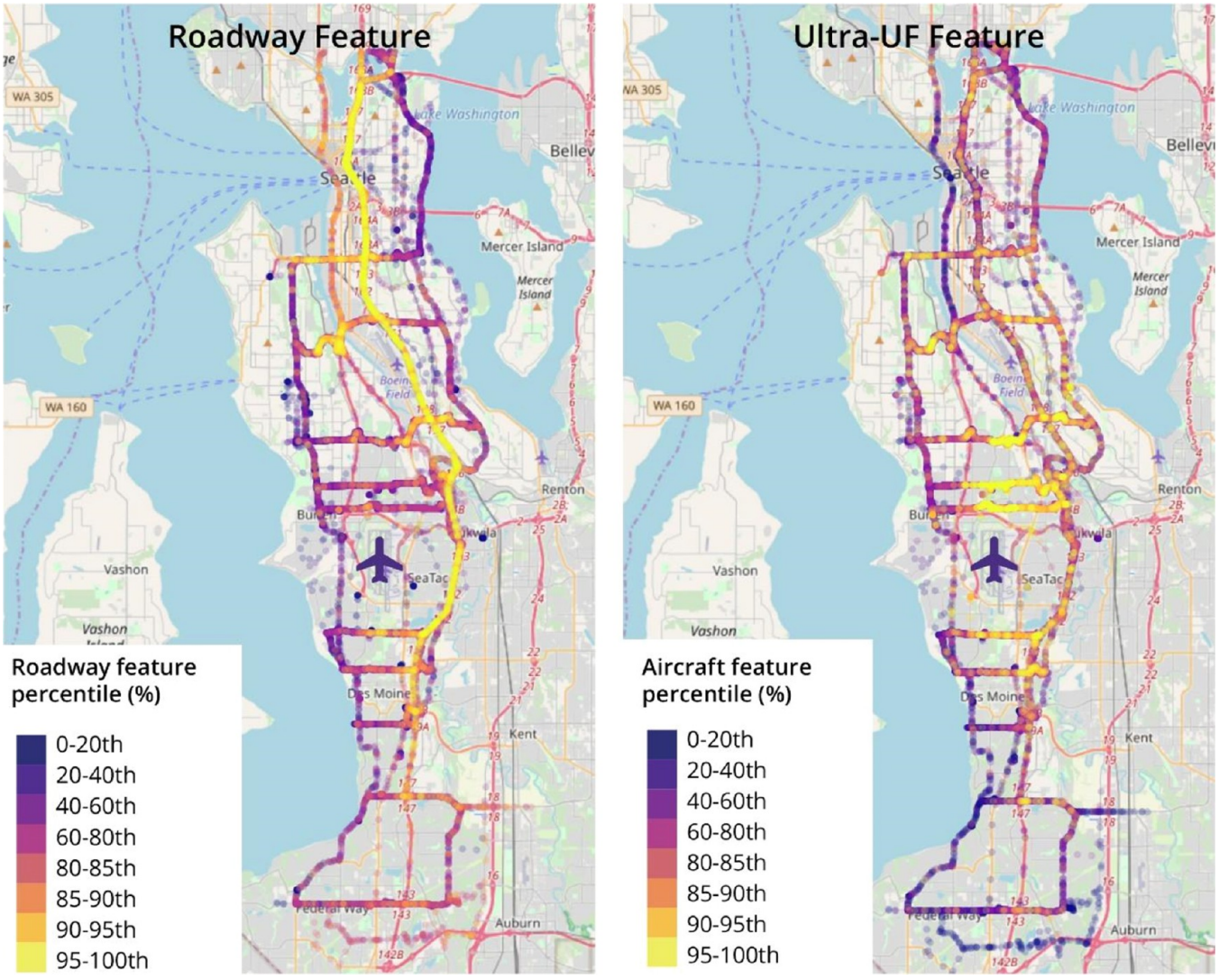

Figure 3. Spatial distribution of the "Ultra-UF" and "roadway" features. Colors correspond to percentile values for each factor score. Percentiles range from 0th percentile representing the smallest observed value to 100th representing the largest observed value.

and southwest. There are fewer time periods with winds exceeding 6 m/s during the north flow operations for our sampled data.

We compared the overall concentration of roadway pollutants, on our transects, on I-5, and on SR-99 (Table S5), along with the total sampling time (in minutes) along each route segment. For the particles and gases measured, we reported the highest mean values on roads, both I-5 and SR 99.

The mean concentration of black carbon observed on I-5 was 5.0 $\mu g/m^3$ with a standard deviation (SD) of 4.3 $\mu g/m^3$, whereas on transect N1 and S1, directly adjacent to the airport on north and south ends, respectively, the mean concentration of black carbon was 1.0 (SD = 1.0) $\mu g/m^3$ and 1.5 (SD = 5.1) $\mu g/m^3$, respectively. The total particle concentration measured on I-5 was 59,896 (37,704) $\#/cm^3$, which is significantly higher than concentrations observed along transects.

It is important to consider that each transect traverses along its east-west length from areas below low aircraft volume to high flight volume. Therefore, summary statistics across the entire transect may not capture peak variations. Typically, the highest SD values are found on the road, although there are some transects that demonstrate more change in pollutant measures.

There was a distinction between the distribution of black carbon and the total particle number (>10 nm) obtained from the two roadway locations and I-5 (Figure 1). Traffic-related pollutants most heavily impacted the high traffic interstate location; however, extreme values (>than the 95th percentile of the data) are common on both the transect and SR 99 sites.

The spatial distribution of traffic-related pollutants confirms that their locations are primarily on and near the major roadways. There is a clear decrease in traffic-related concentrations as the mobile monitoring platform moves away from the high-traffic locations (Figure S3).

3.2. Principal Component Analysis. The PCA yielded two features that together accounted for 61% of the variability in the mobile monitoring data. Figure 2 shows the factor loadings for each feature. These loadings correspond to the correlation coefficients between the pollutant variables and PCA factors. The squared factor loading is the percent of the variance in that variable explained by the factor. Large positive loadings correspond to variables that have a large proportion of

https://dx.doi.org/10.1021/acs.est.0c05933
Environ. Sci. Technol. 2021, 55, 2847−2858

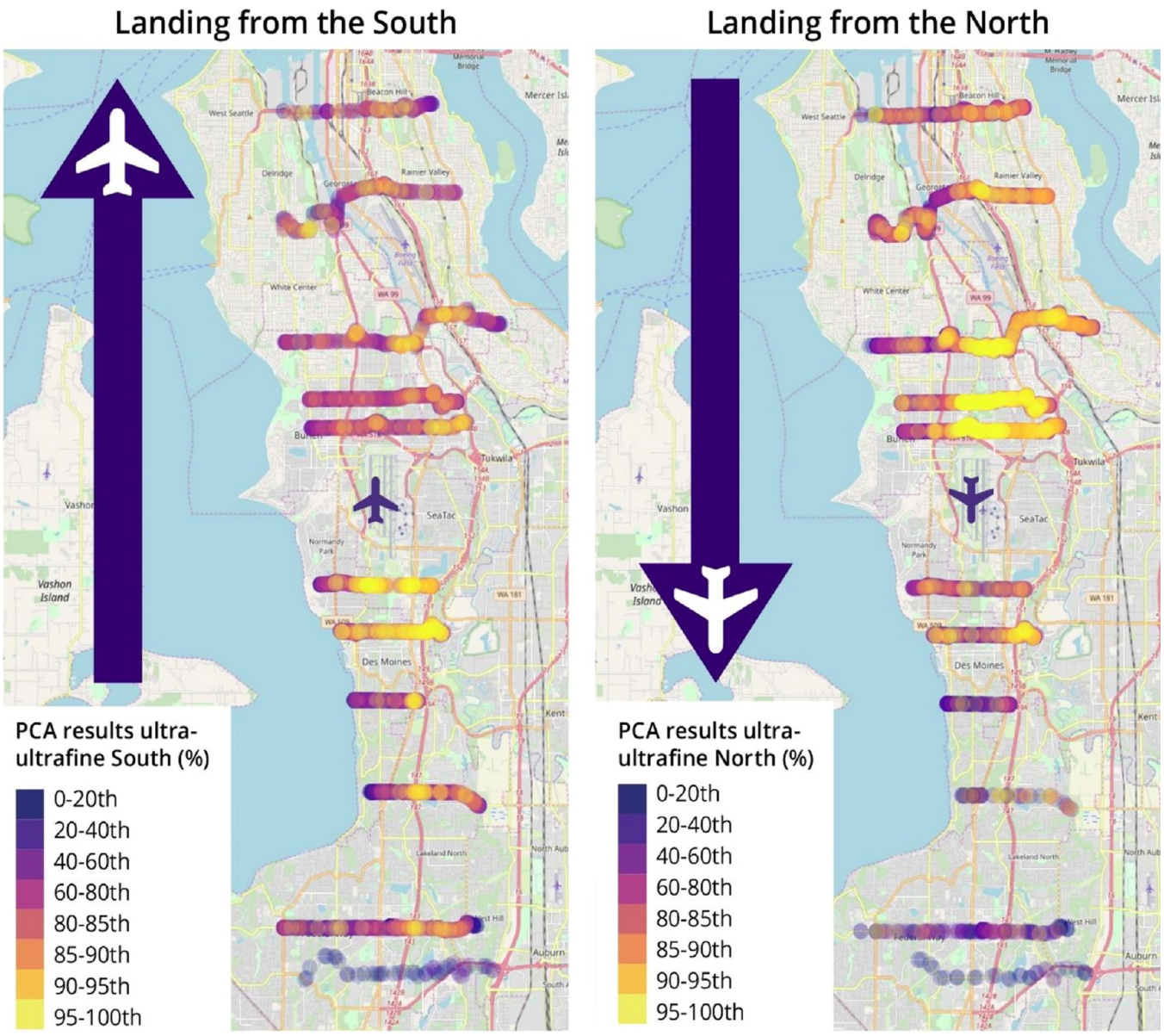

Figure 4. Spatial distribution of the "Ultra-UF" PCA feature, separated by the landing direction. Colors correspond to percentile values for the Ultra-UF factor score. Map layer OpenStreetMap contributors.

their variability captured within the factor. Negative loadings correspond to factors that vary inversely with the factor.

The first feature (RC1) was positively correlated with particles between 10 and 36 nm in diameter. In addition, this feature had a negative correlation with black carbon, a pollutant primarily emitted from diesel combustion, as well as other urban sources such as rail, maritime, manufacturing, and wood heating. When compared to a restricted analysis that included size-resolved information from the NanoScan (Figure S4), there was a correlation of 0.82 between this feature and the NanoScan-based feature with a high proportion of 11.5 and 15.4 nm particles. This same feature had a poor association with particles greater than 20.4 nm. Based on these characteristics, we describe this as the "Ultra-UF feature".

The second feature (RC2) from this analysis has a high correlation with particles between 20 and 36 nm and BC and total UFP concentrations. In contrast, this feature is inversely correlated with particles with a diameter smaller than 20 nm. When compared to a restricted analysis that included size-resolved information (Figure S4), we demonstrated a correlation of 0.79 between this feature and the feature composed of a high proportion of particles between 20 and 36 nm. Based on these characteristics, we described this feature as the "roadway feature".

Figure 3 shows the spatial distribution of these distribution factors and plots the percentile values of the PCA scores computed over the year of sampling for each location we sampled during the mobile monitoring campaign. We can see that the roadway feature, characterized by strong correlations with roadway related pollutants, is the highest overall on I-5 and at major junctions with SR-99. The Ultra-UF feature is not characterized by high concentrations on roadway. This feature shows high values north and south of the airport.

This PCA analysis suggests that based on a mobile monitoring campaign, we can distinguish between roadway-related UFP sources and a distinct UFP source composed primarily of particles less than 20 nm in diameter. Based on the previous literature,[32] this fraction is likely associated with

https://dx.doi.org/10.1021/acs.est.0c05933
Environ. Sci. Technol. 2021, 55, 2847−2858

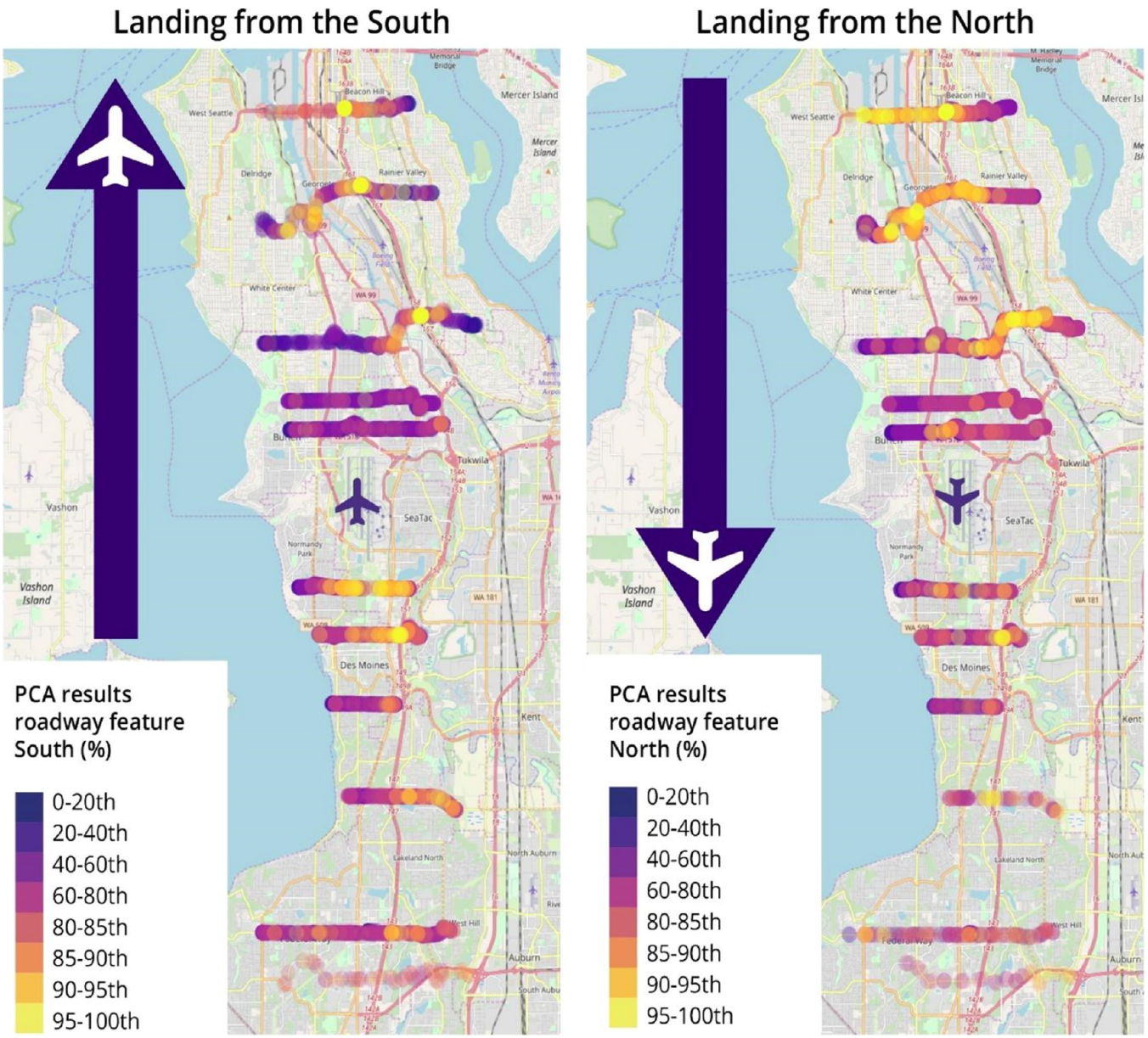

Figure 5. Spatial distribution of the "roadway" feature, separated by the landing direction. Colors correspond to percentile values for the roadway factor score. Map layer OpenStreetMap contributors.

aircraft emissions when aircraft engines are relatively under light load, such as landing. To test the hypothesis that the Ultra-UF feature was associated with periods of time when aircrafts were landing overhead, we separated the data set by the aircraft landing direction.

A high percentage of mobile monitoring measurements underneath the landing path of aircraft were consistent with the Ultra-UF feature (Figure 4). There are still some areas opposite to the landing that show some high PCA scores; these may be due to emissions from aircraft takeoffs or sometimes from a poor separation between traffic and aircraft emissions by the PCA.

In contrast, plotting the scores of the roadway feature by the aircraft landing direction shows (Figure 5) that there is no significant impact of the landing direction on the spatial distribution of this PCA score. A clear spatial gradient east and west of high-traffic roadways in this mapping also emerges. Because of the association with the aircraft landing paths, rather than roadways, the Ultra-UF is likely due to pollution from aircraft emissions.

3.3. Emission Factors. We calculated fuel-based emission factors and grouped them by quantiles of the roadway and Ultra-UF PCA features. This emission factor represents the concentration of particles emitted per kg of fuel burned. In this study, we estimated the emission factor by the ratio of the change in particle number (10−20 nm) to the change in CO_2 associated with each feature. The Methods section describes this calculation in detail. Over the study area, the calculated EF for the roadway feature does not significantly change (Figure 6A). However, the EF at locations with a high aircraft PCA score shows a much higher emission of 10−20 nm particles than locations with a low aircraft PCA score. A Wilcoxon rank sum test confirmed statistically significant differences in UFP emissions between the two pollutant features ($p < 2.2 \times 10^{-16}$) with estimated increased UFP emission of the aircraft feature of 2.9×10^{14} [2.5×10^{14} and 3.3×10^{14}] particles/kg fuel.

https://dx.doi.org/10.1021/acs.est.0c05933
Environ. Sci. Technol. 2021, 55, 2847−2858

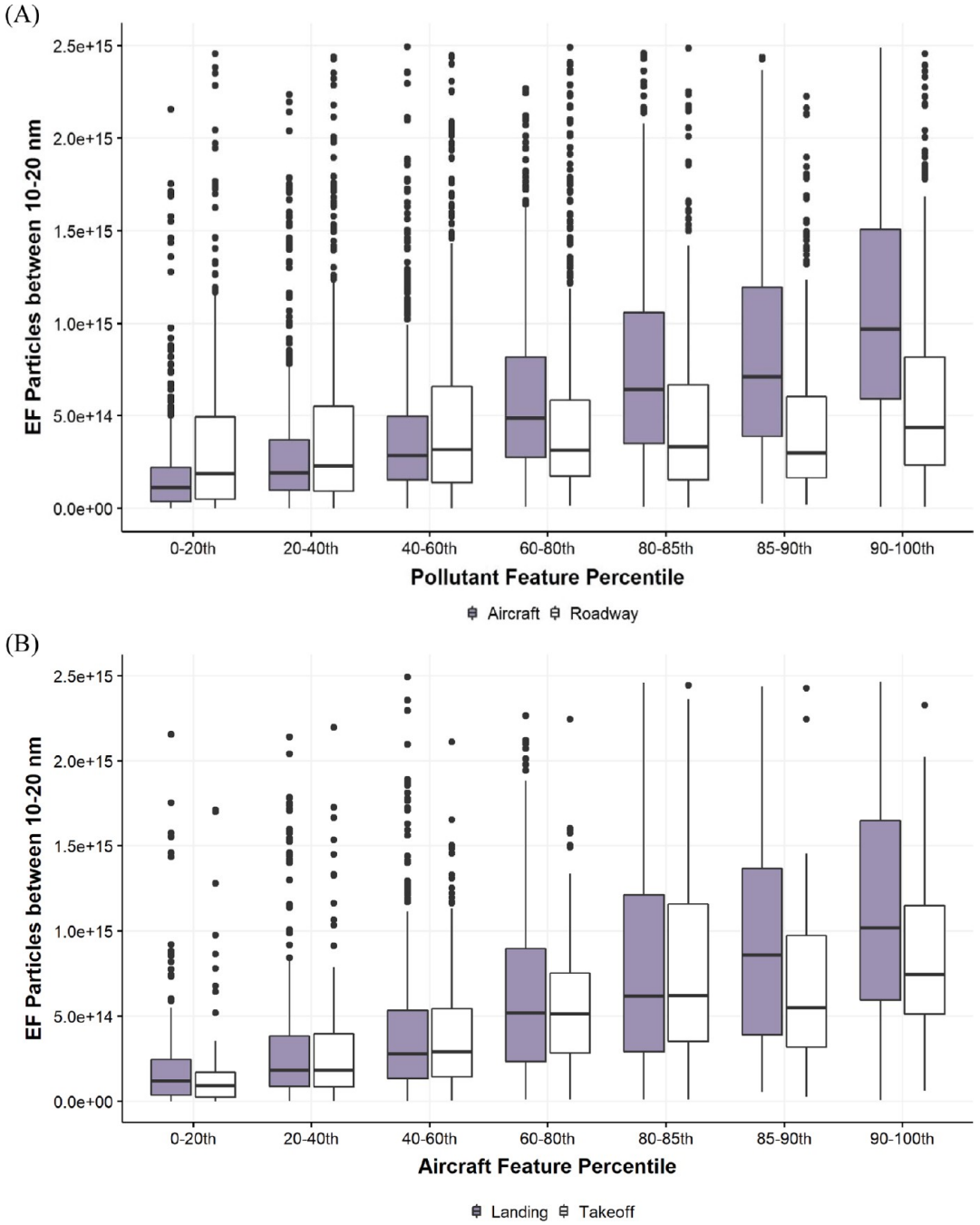

Figure 6. (A) Fuel-based emission factors calculated for quantiles of the PCA scores for the aircraft and roadway features. (B) Fuel-based emission factors calculated only for the aircraft feature for landing and takeoff conditions. Units of the EF are in #particles/kg fuel burned.

Figure 6B further examines the impact of the landing direction on the calculated EF of the aircraft score. A clear difference in emissions is identified for samples under the landing path. The difference between the EF of landing and takeoff conditions is highly significant ($p < 0.01$) and estimated to be 1.4×10^{14} [3.62×10^{13} and 2.5×10^{14}] particles/kg fuel burned based on the Wilcoxon sum test.

4. DISCUSSION

This is the first study that distinguishes between roadway versus aircraft sources of UFP upwind and downwind of a major international airport by exploiting multivariate source features derived from measurements taken on a moving platform. Using multiple pollutant measures taken with this platform throughout the year, we were able to distinguish aircraft-related UFPs from roadway-related UFPs. While UFPs are emitted from both roadway traffic and aircraft and the total number concentration of UFPs (ranging from 10 to 1000 nm) do not distinguish roadway traffic from aircraft, we could separate the pollution from the two sources using measurements of particle size and BC concentrations.

From a multipollutant PCA analysis of mobile monitoring data, we observed two features that explained the majority (61%) of the variance in the pollutant measurements. One of these features is related to roadway traffic, which consisted of relatively larger UFP sizes and high BC concentrations. The

https://dx.doi.org/10.1021/acs.est.0c05933
Environ. Sci. Technol. 2021, 55, 2847−2858

other feature, which we termed Ultra-UF, consisted of relatively smaller UFP sizes and lower BC concentrations. By mapping the locations of the relative contributions of each feature, we observed that the roadway feature was located on and very near the major roadways in the study area, such as I-5 and SR-99. In contrast, we observed the Ultra-UF feature below the landing paths of the aircraft. The PCA did not identify other potential sources of BC and UFPs in our region, namely, seasonal residential wood smoke. This is likely because sampling was distributed throughout the year and designed to be in proximity to roadway and aircraft sources.

Finally, after computing fuel-based emission factors based on the mobile monitoring data, we observed that measurements that were most consistent with the Ultra-UF feature and landing aircraft tended to have a higher emission rate of small 10−20 nm-sized particles per kg of fuel burned compared to measurements that were characterized as roadway feature particles. We computed significantly higher Ultra-UF particle emission per kg fuel burned under landing conditions as compared to takeoff conditions.

Our findings are consistent with previous literature on the roadway and aircraft-related UFP pollution. Monitoring campaigns conducted in airport communities near Los Angeles,[31−33] Atlanta,[34] Boston,[35,36] New York,[37] and Amsterdam[38] have all identified elevated levels of UFPs that the aircrafts have caused. The Los Angeles studies, in particular, found elevated concentrations of UFPs underneath the aircraft landing paths of the LAX airport and that concentrations of UFPs at the ground level near the airport runway tend to consist of smaller 10−20 nm size fractions.[35]

Moreover, our estimates of the emission factor of particles from the aircraft-related Ultra-UF feature are consistent with previous studies that range in magnitude from 10^{14} to 10^{17} particles/kg fuel.[39] Also consistent with previous literature, we estimate a larger UFP impact related to aircraft landings as compared to aircraft takeoffs. This is consistent with previous studies directly testing the emission factors from jet engines at different load conditions and reporting higher emissions of smaller particles under low load conditions.[50] Although this question of the community level impact of landings versus takeoffs is not yet fully established, we believe that our results demonstrate substantial enrichment of Ultra-UF particles, on the order of 10^{14} Ultra-UF/kg_{fuel}, during landing conditions. We recognize that our results do not reflect observations made in previously reported studies[40,43] and hypothesize that some of these differences are related to the instrument cut point (capturing the 10−20 nm range is critical) and sampling design (our study was designed to capture community impacts, not near-runway impacts).

The spatial patterns we observed for the roadway feature UFPs are also consistent with previous studies. Most studies have observed elevated concentrations immediately adjacent to and downwind of major freeways.[51] From these previous studies, UFP concentrations have been found to follow a "rapid decay" spatial pattern with a decrease in concentration by at least 50% over a distance of 150 m away from the major roadway, with a gradual decay to the background thereafter over a distance of 500 m. We observed similar spatial patterns for the roadway PCA feature, which was most associated with measurements on and immediately next to the major roadways in our study area, I-5 and SR-99.

There is a relatively rapid downward transport of these aircraft-emitted UFPs and relatively little time for their physical aging due to coagulation with larger particles. This downward transport is due to a combination of large-scale daytime, convective velocities of up to 1 m/s, and local-scale wingtip vortices that can extend vertically downward for several hundred meters at similar, superimposed velocities.[52] This results in plumes from the descending aircraft during the daytime reaching the ground level in approximately a few minutes near the airport and up to 15 to 20 min at 15 km downwind from the airport.

At these plume transport times, 10−20 nm UFPs emitted by jet engines have a characteristic coagulation half-life of about an hour, assuming that they are emitted into a background aerosol with a number concentration of 1×10^4 particles per cubic centimeter and a count mean diameter of 0.2 μm.[53] It is not surprising that the typical size of these UFPs in the downwind footprint is typically between 10 and 30 nm, indicating minimal coagulation losses.

The differences in the spatial extent of the aircraft versus roadway traffic UFPs are important to consider from a population impact perspective. We observed concentrations of total UFPs (10−1000 nm sized particles) to be higher near roadway compared to our near-airport transects. However, most people spend a relatively small proportion of their time on a major roadway (e.g., during commuting), and because of the relatively short distances over which the roadway UFP decays downwind of major roadways, the roadway UFP would affect only a narrow swath of near-roadway residences and other buildings.

In contrast, the affected areas experiencing elevated aircraft UFPs tend to be more diffuse with consistently elevated concentrations occurring in locations below the decent path of the aircraft. Therefore, considering the map shown in Figure 4, there is the potential for more people to be affected by UFPs from the aircraft than from roadway sources, albeit at lower concentrations. Moreover, those living within the area affected by landing aircraft emissions may be exposed to relatively higher concentrations of smaller sized Ultra-UFPs. There is an urgent need to address this problem because it disproportionately affects communities of color. We overlaid US Census ACS data with Sea-Tac flight paths and the I-5 freeway corridor and observed that approximately 22% of the population of King County lives in proximity to potentially elevated concentrations of UFPs (Table 1). Moreover, the proportion of People of Color is greater in areas of UFP exposure, indicating that this is an alarming new Environmental and Racial Justice issue.

Few epidemiologic studies assess the associations between aircraft UFP exposure and health. One study of two specific locations in Los Angeles observed that short-term exposure to

Table 1[a]

Demographic Characteristics	Population	White	Nonwhite
King county	2,163,257 (100%)	1,404,974 (65%)	728,283 (35%)
within 1 km of the flight paths	188,922 (100%)	84,150 (45%)	104,722 (55%)
within 0.5 km of I-5 freeway	370,964 (100%)	205,278 (55%)	165,686 (45%)
within either 1 km of flight paths or 0.5 km of I-5	468,808 (100%)	254,419 (54%)	214,389 (46%)

[a]5 year US Census American Community Survey (ACS) 2014−2018 tract data.

https://dx.doi.org/10.1021/acs.est.0c05933
Environ. Sci. Technol. 2021, 55, 2847−2858

aircraft-related UFPs is associated with elevated systemic inflammation (IL-6), whereas roadway traffic is more associated with impaired respiratory health (lower FEV_1) and inflammation (elevated sTNFrII).[54] A recent population-based cohort study of all mothers who gave birth from 2008 through 2016 while living within 15 km of LAX found that in utero exposure to aircraft-origin UFPs was positively associated with preterm birth independent of the effects of traffic-related exposures.[55] This suggests that the health effects of aircraft-related UFP exposure may be distinct from roadway traffic UFP exposure, again highlighting the importance of being able to distinguish between sources of UFPs in community settings.

Some of the findings of this study are subject to limitations and uncertainties inherent to a scientific study, as in the following cases. Although both PCA analysis and the ratio of small (e.g., 10−20 nm) to total UFPs indicate a spatial pattern with aircraft activity, there is no chemical or compositional indicator that these particles are directly related to aircraft activity.

We did not observe any features associated with other potentially important urban sources of UFP, including residential wood-smoke burning, industrial emissions, and atmospheric transformation of gaseous pollutants. The PCA methodology does not a priori exclude any pollutant features.

Important future research directions emerged from this study. Although many studies have identified health effects associated with roadway traffic UFPs, the potential health effects from aircraft-related UFP exposure still need major research. Our study highlights the need to fill this knowledge gap because we observed that the particle size distribution of traffic UFPs is different from aircraft UFPs. Our study suggests that the population in some neighborhoods may have more exposure to UFPs than others due to proximity to roadway traffic or overlap with the plumes from aircraft emissions. Additionally, roadway and aircraft traffic has changed in volume, travel patterns, and per unit emissions over time. It will likely continue to change, creating uncertainties in the impacts of future UFP exposures.

■ ASSOCIATED CONTENT

Supporting Information

The Supporting Information is available free of charge at https://pubs.acs.org/doi/10.1021/acs.est.0c05933.

> Summary of each mobile monitoring transect; summary of instruments used in the MOV-UP study; summary of colocation calibration results for PNC and BC monitors; summary of drive days across the four seasons of the MOV-UP study; summary measures from the mobile monitoring campaign by monitoring the location and transect; MOV-UP study setup; wind rose plots; spatial distribution of traffic-related pollutant concentration percentiles; and principal component factor loadings for each feature of the secondary PCA analyses (PDF)

■ AUTHOR INFORMATION

Corresponding Author

Elena Austin − *Department of Environmental & Occupational Health Sciences, University of Washington, Seattle, Washington 98195, United States;* orcid.org/0000-0002-4724-1042; Phone: 206-221-6301; Email: elaustin@uw.edu

Authors

Jianbang Xiang − *Department of Environmental & Occupational Health Sciences, University of Washington, Seattle, Washington 98195, United States;* orcid.org/0000-0001-5196-2574

Timothy R. Gould − *Department of Civil & Environmental Engineering, University of Washington, Seattle, Washington 98195, United States*

Jeffry H. Shirai − *Department of Environmental & Occupational Health Sciences, University of Washington, Seattle, Washington 98195, United States;* orcid.org/0000-0002-9864-532X

Sukyong Yun − *Department of Civil & Environmental Engineering, University of Washington, Seattle, Washington 98195, United States*

Michael G. Yost − *Department of Environmental & Occupational Health Sciences, University of Washington, Seattle, Washington 98195, United States*

Timothy V. Larson − *Department of Environmental & Occupational Health Sciences, University of Washington, Seattle, Washington 98195, United States*

Edmund Seto − *Department of Environmental & Occupational Health Sciences, University of Washington, Seattle, Washington 98195, United States*

Complete contact information is available at: https://pubs.acs.org/10.1021/acs.est.0c05933

Notes

The authors declare no competing financial interest.

■ ACKNOWLEDGMENTS

The authors wish to express special thanks to Dave Hardie for his efforts in the field work. The study was funded by the State of Washington for the MOV-UP study and Award Number 5P30 ES007033-23 from the National Institute of Environmental Health Sciences.

■ REFERENCES

(1) Ross, M. A. *Integrated Science Assessment for Particulate Matter*; US Environmental Protection Agency: Washington DC, USA, 2009; pp 61−161.

(2) Baldwin, N.; Gilani, O.; Raja, S.; Batterman, S.; Ganguly, R.; Hopke, P.; Berrocal, V.; Robins, T.; Hoogterp, S. Factors affecting pollutant concentrations in the near-road environment. *Atmos. Environ.* **2015**, *115*, 223−235.

(3) Hagler, G. S. W.; Thoma, E. D.; Baldauf, R. W. High-resolution mobile monitoring of carbon monoxide and ultrafine particle concentrations in a near-road environment. *J. Air Waste Manage. Assoc.* **2010**, *60*, 328−336.

(4) Hu, S.; Paulson, S. E.; Fruin, S.; Kozawa, K.; Mara, S.; Winer, A. M. Observation of elevated air pollutant concentrations in a residential neighborhood of Los Angeles California using a mobile platform. *Atmos. Environ.* **2012**, *51*, 311−319.

(5) Levy, I.; Mihele, C.; Lu, G.; Narayan, J.; Hilker, N.; Brook, J. R. Elucidating multipollutant exposure across a complex metropolitan area by systematic deployment of a mobile laboratory. *Atmos. Chem. Phys.* **2014**, *14*, 7173−7193.

(6) Patton, A. P.; Perkins, J.; Zamore, W.; Levy, J. I.; Brugge, D.; Durant, J. L. Spatial and temporal differences in traffic-related air pollution in three urban neighborhoods near an interstate highway. *Atmos. Environ.* **2014**, *99*, 309−321.

(7) Sabaliauskas, K.; Jeong, C.-H.; Yao, X.; Reali, C.; Sun, T.; Evans, G. J. Development of a land-use regression model for ultrafine particles in Toronto, Canada. *Atmos. Environ.* **2015**, *110*, 84−92.

(8) Shairsingh, K. K.; Jeong, C.-H.; Wang, J. M.; Evans, G. J. Characterizing the spatial variability of local and background concentration signals for air pollution at the neighbourhood scale. *Atmos. Environ.* **2018**, *183*, 57−68.
(9) Weichenthal, S.; Van Ryswyk, K.; Goldstein, A.; Shekarrizfard, M.; Hatzopoulou, M. Characterizing the spatial distribution of ambient ultrafine particles in Toronto, Canada: A land use regression model. *Environ. Pollut.* **2016**, *208*, 241−248.
(10) Westerdahl, D.; Wang, X.; Pan, X.; Zhang, K. M. Characterization of on-road vehicle emission factors and microenvironmental air quality in Beijing, China. *Atmos. Environ.* **2009**, *43*, 697−705.
(11) Xiang, J.; Austin, E.; Gould, T.; Larson, T.; Shirai, J.; Liu, Y.; Marshall, J.; Seto, E. Impacts of the COVID-19 responses on traffic-related air pollution in a Northwestern US city. *Sci. Total Environ.* **2020**, *747*, 141325.
(12) Pekkanen, J.; Kulmala, M. Exposure assessment of ultrafine particles in epidemiologic time-series studies. *Scand. J. Work. Environ. Health* **2004**, *30*, 9−18.
(13) Natusch, D. F. S.; Wallace, J. R. Urban aerosol toxicity: the influence of particle size. *Science* **1974**, *186*, 695−699.
(14) Seaton, A.; Godden, D.; MacNee, W.; Donaldson, K. Particulate air pollution and acute health effects. *Lancet* **1995**, *345*, 176−178.
(15) Hoek, G.; Boogaard, H.; Knol, A.; De Hartog, J.; Slottje, P.; Ayres, J. G.; Borm, P.; Brunekreef, B.; Donaldson, K.; Forastiere, F. Concentration response functions for ultrafine particles and all-cause mortality and hospital admissions: results of a European expert panel elicitation. *Environ. Sci. Technol.* **2010**, *44*, 476−482.
(16) Goldberg, M. S.; Labrèche, F.; Weichenthal, S.; Lavigne, E.; Valois, M.-F.; Hatzopoulou, M.; Van Ryswyk, K.; Shekarrizfard, M.; Villeneuve, P. J.; Crouse, D.; Parent, M.-É. The association between the incidence of postmenopausal breast cancer and concentrations at street-level of nitrogen dioxide and ultrafine particles. *Environ. Res.* **2017**, *158*, 7−15.
(17) Bai, L.; Weichenthal, S.; Kwong, J. C.; Burnett, R. T.; Hatzopoulou, M.; Jerrett, M.; van Donkelaar, A.; Martin, R. V.; Van Ryswyk, K.; Lu, H.; Kopp, A.; Chen, H. Associations of Long-Term Exposure to Ultrafine Particles and Nitrogen Dioxide With Increased Incidence of Congestive Heart Failure and Acute Myocardial Infarction. *Am. J. Epidemiol.* **2018**, *188*, 151−159.
(18) Corlin, L.; Ball, S.; Woodin, M.; Patton, A.; Lane, K.; Durant, J.; Brugge, D. Relationship of Time-Activity-Adjusted Particle Number Concentration with Blood Pressure. *Int. J. Environ. Res. Public Health* **2018**, *15*, 2036.
(19) Ostro, B.; Hu, J.; Goldberg, D.; Reynolds, P.; Hertz, A.; Bernstein, L.; Kleeman, M. J. Associations of mortality with long-term exposures to fine and ultrafine particles, species and sources: results from the California Teachers Study Cohort. *Environ. Health Perspect.* **2015**, *123*, 549−556.
(20) Rich, D. Q.; Peters, A.; Schneider, A.; Zareba, W.; Breitner, S.; Oakes, D.; Wiltshire, J.; Kane, C.; Frampton, M. W.; Hampel, R.; Hopke, P. K.; Cyrys, J.; Utell, M. J. Ambient and Controlled Particle Exposures as Triggers for Acute ECG Changes. *Res. Rep.—Health Eff. Inst.* **2016**, *186*, 5−75.
(21) Weichenthal, S.; Hatzopoulou, M.; Goldberg, M. S. Exposure to traffic-related air pollution during physical activity and acute changes in blood pressure, autonomic and micro-vascular function in women: a cross-over study. *Part. Fibre Toxicol.* **2014**, *11*, 70.
(22) Weichenthal, S.; Lavigne, E.; Valois, M.-F.; Hatzopoulou, M.; Van Ryswyk, K.; Shekarrizfard, M.; Villeneuve, P. J.; Goldberg, M. S.; Parent, M.-E. Spatial variations in ambient ultrafine particle concentrations and the risk of incident prostate cancer: A case-control study. *Environ. Res.* **2017**, *156*, 374−380.
(23) Weichenthal, S.; Bai, L.; Hatzopoulou, M.; Van Ryswyk, K.; Kwong, J. C.; Jerrett, M.; van Donkelaar, A.; Martin, R. V.; Burnett, R. T.; Lu, H. Long-term exposure to ambient ultrafine particles and respiratory disease incidence in in Toronto, Canada: a cohort study. *Environ. Health* **2017**, *16*, 64.
(24) Cass, G. R.; Hughes, L. A.; Bhave, P.; Kleeman, M. J.; Allen, J. O.; Salmon, L. G. The chemical composition of atmospheric ultrafine particles. *Proc. R. Soc. London, Ser. A* **2000**, *358*, 2581−2592.
(25) Fruin, S.; Westerdahl, D.; Sax, T.; Sioutas, C.; Fine, P. M. Measurements and predictors of on-road ultrafine particle concentrations and associated pollutants in Los Angeles. *Atmos. Environ.* **2008**, *42*, 207−219.
(26) Hagler, G. S. W.; Baldauf, R. W.; Thoma, E. D.; Long, T. R.; Snow, R. F.; Kinsey, J. S.; Oudejans, L.; Gullett, B. K. Ultrafine particles near a major roadway in Raleigh, North Carolina: Downwind attenuation and correlation with traffic-related pollutants. *Atmos. Environ.* **2009**, *43*, 1229−1234.
(27) Holmén, B. A.; Ayala, A. Ultrafine PM emissions from natural gas, oxidation-catalyst diesel, and particle-trap diesel heavy-duty transit buses. *Environ. Sci. Technol.* **2002**, *36*, 5041−5050.
(28) Larson, T.; Gould, T.; Riley, E. A.; Austin, E.; Fintzi, J.; Sheppard, L.; Yost, M.; Simpson, C. Ambient air quality measurements from a continuously moving mobile platform: Estimation of area-wide, fuel-based, mobile source emission factors using absolute principal component scores. *Atmos. Environ.* **2017**, *152*, 201−211.
(29) Riley, E. A.; Banks, L.; Fintzi, J.; Gould, T. R.; Hartin, K.; Schaal, L.; Davey, M.; Sheppard, L.; Larson, T.; Yost, M. G.; Simpson, C. D. Multi-pollutant mobile platform measurements of air pollutants adjacent to a major roadway. *Atmos. Environ.* **2014**, *98*, 492−499.
(30) Zhu, Y.; Hinds, W. C.; Kim, S.; Shen, S.; Sioutas, C. Study of ultrafine particles near a major highway with heavy-duty diesel traffic. *Atmos. Environ.* **2002**, *36*, 4323−4335.
(31) Hsu, H.-H.; Adamkiewicz, G.; Houseman, E. A.; Zarubiak, D.; Spengler, J. D.; Levy, J. I. Contributions of aircraft arrivals and departures to ultrafine particle counts near Los Angeles International Airport. *Sci. Total Environ.* **2013**, *444*, 347−355.
(32) Hudda, N.; Gould, T.; Hartin, K.; Larson, T. V.; Fruin, S. A. Emissions from an international airport increase particle number concentrations 4-fold at 10 km downwind. *Environ. Sci. Technol.* **2014**, *48*, 6628−6635.
(33) Hudda, N.; Fruin, S. A. International airport impacts to air quality: size and related properties of large increases in ultrafine particle number concentrations. *Environ. Sci. Technol.* **2016**, *50*, 3362−3370.
(34) Riley, E. A.; Gould, T.; Hartin, K.; Fruin, S. A.; Simpson, C. D.; Yost, M. G.; Larson, T. Ultrafine particle size as a tracer for aircraft turbine emissions. *Atmos. Environ.* **2016**, *139*, 20−29.
(35) Hudda, N.; Simon, M. C.; Zamore, W.; Brugge, D.; Durant, J. L. Aviation emissions impact ambient ultrafine particle concentrations in the greater Boston area. *Environ. Sci. Technol.* **2016**, *50*, 8514−8521.
(36) Hudda, N.; Simon, M. C.; Zamore, W.; Durant, J. L. Aviation-Related impacts on ultrafine particle number concentrations outside and inside residences near an airport. *Environ. Sci. Technol.* **2018**, *52*, 1765−1772.
(37) Masiol, M.; Hopke, P. K.; Felton, H. D.; Frank, B. P.; Rattigan, O. V.; Wurth, M. J.; LaDuke, G. H. Analysis of major air pollutants and submicron particles in New York City and Long Island. *Atmos. Environ.* **2017**, *148*, 203−214.
(38) Keuken, M. P.; Moerman, M.; Zandveld, P.; Henzing, J. S.; Hoek, G. Total and size-resolved particle number and black carbon concentrations in urban areas near Schiphol airport (the Netherlands). *Atmos. Environ.* **2015**, *104*, 132−142.
(39) Shirmohammadi, F.; Sowlat, M. H.; Hasheminassab, S.; Saffari, A.; Ban-Weiss, G.; Sioutas, C. Emission rates of particle number, mass and black carbon by the Los Angeles International Airport (LAX) and its impact on air quality in Los Angeles. *Atmos. Environ.* **2017**, *151*, 82−93.
(40) Stacey, B.; Harrison, R. M.; Pope, F. Evaluation of ultrafine particle concentrations and size distributions at London Heathrow Airport. *Atmos. Environ.* **2020**, *222*, 117148.
(41) Lopes, M.; Russo, A.; Monjardino, J.; Gouveia, C.; Ferreira, F. Monitoring of ultrafine particles in the surrounding urban area of a civilian airport. *Atmos. Pollut. Res.* **2019**, *10*, 1454−1463.

https://dx.doi.org/10.1021/acs.est.0c05933
Environ. Sci. Technol. 2021, 55, 2847−2858

(42) Tessum, M. W.; Larson, T.; Gould, T. R.; Simpson, C. D.; Yost, M. G.; Vedal, S. Mobile and fixed-site measurements to identify spatial distributions of traffic-related pollution sources in Los Angeles. *Environ. Sci. Technol.* **2018**, *52*, 2844−2853.
(43) Rivas, I.; Beddows, D. C. S.; Amato, F.; Green, D. C.; Järvi, L.; Hueglin, C.; Reche, C.; Timonen, H.; Fuller, G. W.; Niemi, J. V.; Pérez, N.; Aurela, M.; Hopke, P. K.; Alastuey, A.; Kulmala, M.; Harrison, R. M.; Querol, X.; Kelly, F. J. Source apportionment of particle number size distribution in urban background and traffic stations in four European cities. *Environ. Int.* **2020**, *135*, 105345.
(44) Masiol, M.; Vu, T. V.; Beddows, D. C. S.; Harrison, R. M. Source apportionment of wide range particle size spectra and black carbon collected at the airport of Venice (Italy). *Atmos. Environ.* **2016**, *139*, 56−74.
(45) Austin, E.; Xiang, J.; Gould, T.; Shirai, J.; Yun, S.; Yost, M.; Larson, T.; Seto, E. *Mobile ObserVations of Ultrafine Particles: The MOV-UP Study Report*; University of Washington: Seattle, WA, 2019.
(46) Iowa Environmental Mesonet, ASOS Network. https://mesonet.agron.iastate.edu/request/download.phtml?network=WA_ASOS (May 20, 2020).
(47) Xiang, J.; Austin, E.; Gould, T.; Larson, T.; Yost, M.; Shirai, J.; Liu, Y.; Yun, S.; Seto, E. Using vehicles' rendezvous for in-situ calibration of instruments in fleet vehicle-based air pollution mobile monitoring. *Environ. Sci. Technol.* **2020**, *54*, 4286−4294.
(48) Hagler, G. S. W.; Yelverton, T. L. B.; Vedantham, R.; Hansen, A. D. A.; Turner, J. R. Post-processing method to reduce noise while preserving high time resolution in aethalometer real-time black carbon data. *Aerosol Air Qual. Res.* **2011**, *11*, 539−546.
(49) Yacovitch, T. I.; Yu, Z.; Herndon, S. C.; Miake-Lye, R.; Liscinsky, D.; Knighton, W. B.; Kenney, M.; Schoonard, C.; Pringle, P. *Exhaust Emissions from In-Use General Aviation Aircraft*; Transportation Research Board, 2016, 7 (1), 35−56.
(50) Jonsdottir, H. R.; Delaval, M.; Leni, Z.; Keller, A.; Brem, B. T.; Siegerist, F.; Schönenberger, D.; Durdina, L.; Elser, M.; Burtscher, H. Non-volatile particle emissions from aircraft turbine engines at ground-idle induce oxidative stress in bronchial cells. *Commun. Biol.* **2019**, *2*, 90.
(51) Karner, A. A.; Eisinger, D. S.; Niemeier, D. A. Near-roadway air quality: synthesizing the findings from real-world data. *Environ. Sci. Technol.* **2010**, *44*, 5334−5344.
(52) Graham, A.; Raper, D. Transport to ground of emissions in aircraft wakes. Part I: Processes. *Atmos. Environ.* **2006**, *40*, 5574−5585.
(53) Seinfeld, J. H.; Pandis, S. N. From air pollution to climate change. *Atmos. Chem. Phys.* **1998**, *51*, 88.
(54) Habre, R.; Zhou, H.; Eckel, S. P.; Enebish, T.; Fruin, S.; Bastain, T.; Rappaport, E.; Gilliland, F. Short-term effects of airport-associated ultrafine particle exposure on lung function and inflammation in adults with asthma. *Environ. Int.* **2018**, *118*, 48−59.
(55) Wing, S. E.; Larson, T. V.; Hudda, N.; Boonyarattaphan, S.; Fruin, S.; Ritz, B. Preterm Birth among Infants Exposed to in Utero Ultrafine Particles from Aircraft Emissions. *Environ. Health Perspect.* **2020**, *128*, 047002.

https://dx.doi.org/10.1021/acs.est.0c05933
Environ. Sci. Technol. 2021, 55, 2847−2858